UNIVERSITY OF AMSTERDAM

UvA-DARE (Digital Academic Repository)

Spatial correlations and deformation modes in sheared colloidal glasses

Chikkadi, V.K.

Publication date
2011

Citation for published version (APA):
Chikkadi, V. K. (2011). *Spatial correlations and deformation modes in sheared colloidal glasses*. [Thesis, fully internal, Universiteit van Amsterdam].

4 Long-range strain correlations in sheared colloidal glasses

Glasses behave as solids due to their long relaxation time; the origin of this slow response remains a puzzle. Growing dynamic length scales due to cooperative motion of particles are believed to be central to the understanding of such slow response and the emergence of rigidity [93, 94]. However, for quiescent glasses, the size of the cooperatively rearranging regions has never been observed to exceed a few particle diameters [95, 96], and the observation of long-range correlations that are signatures of an elastic solid has remained elusive. Here, we provide direct experimental evidence of long-range correlations in a dense colloidal glass by imposing an external stress on the system, forcing structural rearrangements that make the glass flow. We identify long-range correlations in the fluctuations of microscopic strain, and elucidate their scaling and spatial symmetry. The long-range correlations are observed to lead to inhomogeneous flow when the flow becomes so fast that the structural rearrangements can no longer occur through spontaneous thermal fluctuations.
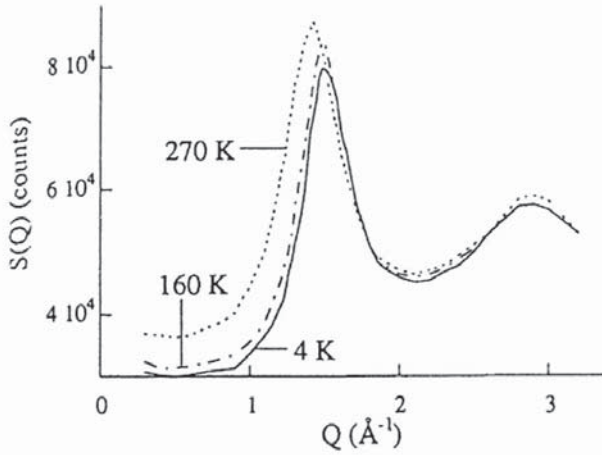
Figure 4.1: Static structure factor of liquid ($T = 270K$) and glassy ($T = 160K$, $T = 4$) polybutadiene at ambient pressure is plotted vs. wave-vector, as obtained from the neutron scattering measurement [97, 98].

4.1 Correlations in glasses

4.1.1 Static two point correlations

Various atomic or polymeric liquids, when cooled rapidly form an amorphous solid known as a glass [1]. On approach to the glass transition, a liquid does not display any perceptible change in structure, however, the dynamics slows down dramatically [9]. A simple static measure of the structure is the two-point correlation function or the structure factor, which is defined as

$$S(q) = \left\langle \frac{1}{N} \rho_{\mathbf{q}} \rho_{-\mathbf{q}} \right\rangle, \tag{4.1}$$

where the Fourier component of density is written as $\rho_q = \sum_{j=1}^{N} \exp\left(i\mathbf{q}.r_j\right)$, with N the number of particles and r_j the position of the particle j. The structure factor gives information about the density fluctuations on length scales $2\pi/|q|$. However, the change of $S(q)$ in the vicinity of the glass transition is unremarkable, with no hint of a growing length scale. In real space, this correlation function is referred as pair correlation function, which was introduced in Chap. 2. A direct measurement of S(q) at different temperatures in a polybutadiene polymer glass former using neutron scattering is shown in Fig. 4.1 [97, 98].

4.1.2   Dynamic four-point correlations

Simple static correlations, such as the ones discussed in the previous section, are not helpful in understanding the slowing down of the system. Major changes at the glass transition, however, do occur in the dynamics of the particles. The determination of dynamic quantities requires measurement in both time and space. To understand the spatio-temporal dynamics, an observable called *mobility* $c_i(t, 0)$ is defined to measure how far a particle i moves in a time interval t [7, 99]. A corresponding *mobility field* is conveniently defined as :

$$c(r; t, 0) = \sum_i c_i(t, 0)\delta(\mathbf{r} - \mathbf{r}_i). \tag{4.2}$$

Then, the spatial correlations of the mobility are naturally captured through the correlation function

$$G_4(r; t) = \langle c(\mathbf{r}; t, 0)c(\mathbf{0}; t, 0)\rangle - \langle c(\mathbf{r}; t, 0)\rangle^2, \tag{4.3}$$

which is dependent only on a single time t and a separation distance $r = |\mathbf{r}|$, as long as the average is taken at equilibrium in a translational invariant system [7]. The analogy with fluctuations in critical systems becomes clear in Eq.4.3 if one considers the mobility field $c(\mathbf{r}; t, 0)$ as playing the role of the order parameter for the glass transition. The mobility $c_i(t, 0)$ can often be expressed as a two-point function over a distance $2\pi/q$

$$c_i(t, 0) = o_i(\mathbf{q}, t)o_i(-\mathbf{q}, 0), \tag{4.4}$$

where $o_i(\mathbf{q}, t) = \exp(iq.\mathbf{r}_i(t))$ is the Fourier component of the density of the system. Moving from a particle notation $o_i(\mathbf{q}, t)$ to a field notation $o_i(\mathbf{x}; t, 0)$, one arrives at [7, 99]

$$G_4(r; t) = \langle o(\mathbf{r}; \mathbf{q}, t)o(\mathbf{r}; -\mathbf{q}, 0)o(\mathbf{0}; \mathbf{q}, t)o(\mathbf{0}; -\mathbf{q}, 0)\rangle - \langle o(\mathbf{r}; \mathbf{q}, t)o(\mathbf{r}; -\mathbf{q}, 0)\rangle^2. \tag{4.5}$$

This correlation function is quartic in the operator o, so it is known as a *four-point correlation function*. It measures correlations on a length scale r, associated with motion between time zero and time t; it depends additionally on the length scale q used in the definition of the particle mobility $c_i(t, 0)$. Since structural relaxation typically involves particle motion over a distance comparable to the particle size σ, one typically

chooses $q << 1/\sigma$ and studies the remaining t and r dependence. This function then characterizes the dynamic heterogeneity in glasses, and allows the language of field theory and critical phenomena to be used in studying dynamical fluctuations in glassy systems. By analogy with critical phenomena, if there is a single dominant length scale ζ_4 then one expects that for large r, the correlation function decays as

$$G_4(r;t) \sim \frac{A(t)}{r^p} \exp\left(-r/\xi_4(t)\right), \tag{4.6}$$

with p an exponent whose value is discussed below. It is natural to define the susceptibility associated with the correlation function

$$\chi_4(t) = \int dr G_4(r;t). \tag{4.7}$$

The dynamic susceptibility $\chi_4(t)$ is the non-equilibrium analogue of the thermodynamic susceptibility that measures the size of the fluctuations. The size of the fluctuations is directly related to the size of the cooperatively moving clusters of particles [7, 99].

4.2   Numerical and experimental investigation of dynamic correlations

Dynamic correlations have been studied in quiescent glasses both in simulation and experiments [21, 22, 95, 100, 101, 102]. We first briefly describe some of the results to gain an overview of the existing understanding of dynamic correlations in various systems.

4.2.1   Simulation studies

For supercooled liquids, the dynamic susceptibility $\chi_4(t)$ has been measured by molecular dynamics, Brownian and Monte Carlo simulations in different liquids [94, 102, 103, 104, 105, 106, 107]. The qualitative behavior is similar in all cases. An example of the measurement of $\chi_4(t)$ and the associated length scale $\xi_4(t)$ is shown in Fig.4.2(a)&(b), respectively, for a Lennard-Jones liquid [105]. The susceptibility $\chi_4(t)$ and the length scale $\xi_4(t)$ first increases, has a peak on a timescale close to structural
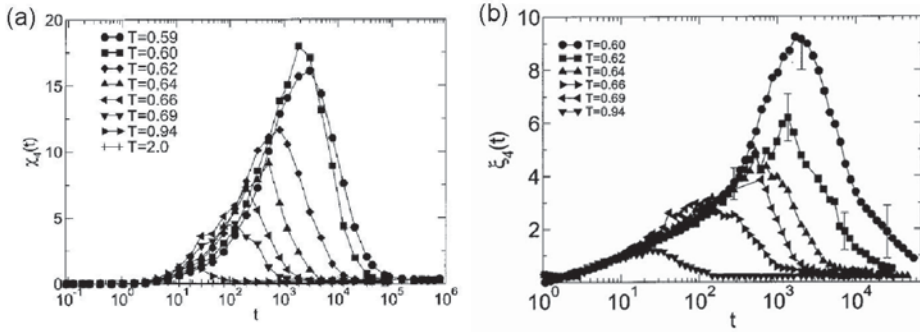
Figure 4.2: Dynamic correlations in computer simulations of supercooled liquids using Lennard-Jones interactions [105]. Time and temperature dependence of (a) $\chi_4(t)$ and (b) $\xi_4(t)$. As T decreases, the peak in $\chi_4(t)$ and $\xi_4(t)$ monotonically increases and shifts to longer time. Both $\chi_4(t)$ and $\xi_4(t)$ attain a maximum at $t \sim \tau_4^{max}$.

relaxation timescale (τ_α) and then decreases. The most important information extracted from the temperature evolution of $\chi_4(t)$ is that, at least in the range available to the numerical simulations, the value of the peak typically increases from a high temperature value that is of order unity, and goes up by at most 2 orders of magnitude at the lowest temperatures for which the system can be equilibrated. This suggests that dynamics becomes increasingly spatially correlated when T decreases.   Dynamic correlations were originally proposed to study cooperative motion on the approach to the glass transition [94, 94, 100, 101, 103, 108, 109]. However, over the last decade, the four-point correlation function $G_4(r)$ (Eq.4.3) has been used extensively to study the cooperative length scales in sheared amorphous solids [49, 110, 111, 112]. An example of the four-point correlation function measured in athermal, quasi-static simulations of the deformation of amorphous solids is shown in Fig. 4.3 [49]. The spatial correlations of the non-affine displacements are shown for various system sizes in Fig. 4.3. These results indicate that there is no characteristic length scale due to the elastic nature of the system, and the only relevant scale is the system size.
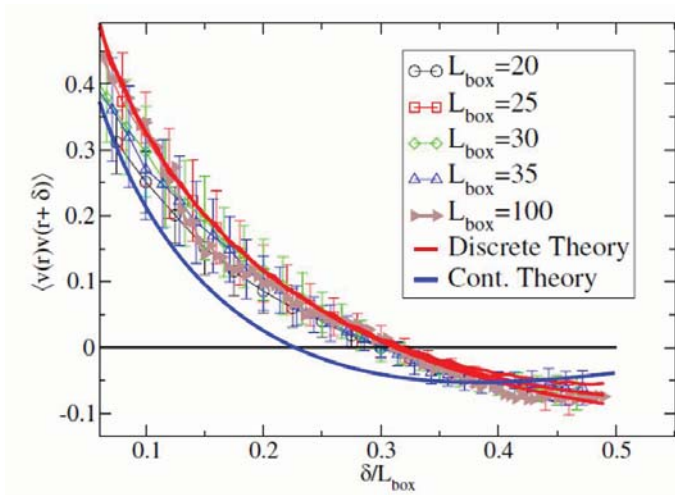
Figure 4.3: Spatial correlations of the non-affine displacements in athermal, quasi-static simulation of deformation in amorphous solids [49]. The separation distance δ on the x-axis is scaled by the system size L_{box}.
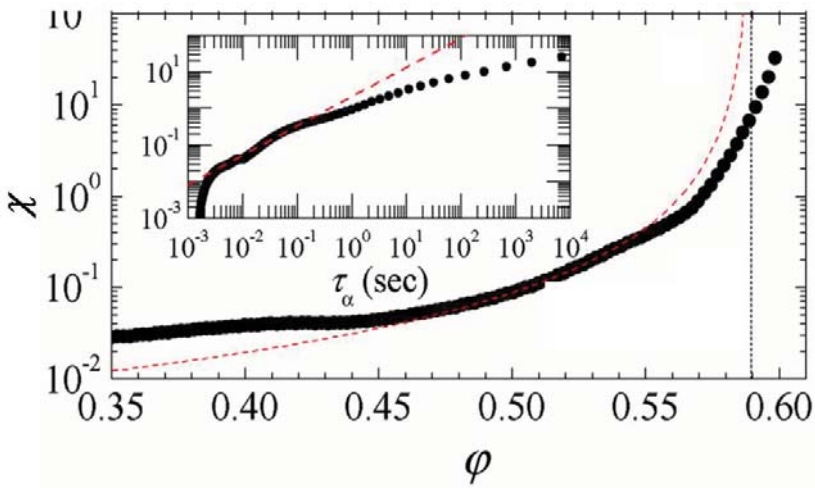

Figure 4.4: Measurement of dynamic susceptibility in dense colloidal suspensions using dynamic light scattering [13]. The peak of $\chi_4(t)$ is shown as a function of the volume fractions. The inset shows the peak of $\chi_4(t)$ as a function of the structural relaxation time τ_α.

4.2.2   Experimental studies

In experiments, dynamic correlations have been measured in hard-sphere colloidal suspensions using the technique of dynamic light scattering [13, 95]. Examples of the susceptibility $\chi_4(t)$ and the associated correlation length $\xi_4(t)$ measured by Brambilla and co-workers [13] are shown in Fig.4.4. These results are qualitatively similar to what has been observed in simulations [94, 102, 103, 104, 105, 106, 107]. Direct observations of particle motion can be made in dense colloidal glasses using confocal microscopy. The four-point correlation function $G_4(r)$ was measured using the displacement of the particles in quiescent colloidal glasses [96]. However, these authors did not discuss the dynamic nature of the correlation function $G_4(r)$. Other examples of experimental determinations of dynamic correlations are excited granular materials [21, 113] and coarsening foams [114]. The results obtained in all these cases are again broadly similar for the time dependence of $\chi_4(t)$.

4.3   Probability distribution of non-affine displacement fluctuations

In order to understand the correlated dynamics in glasses, we begin with the investigation of the probability distribution function of non-affine displacements Δr^{na}, which is defined according to Eq. 2.11. It suffices to analyze only the component in the shear direction, Δx^{na}. As discussed previously, the correlations in glasses are time dependent because they are strongly out of equilibrium. To illustrate this time dependence, we determine non-affine displacements over different time intervals. In Fig.4.5(a), we show the probability distributions of non-affine displacements obtained at a shear rate of $\dot{\gamma} = 1 \times 10^{-5} s^{-1}$ and $\phi = 0.60$. The probability distributions are normalized such that they have zero mean and unit variance, and the maximum of the function is set to unity. The circular and square symbols in Fig.4.5(a) are used to distinguish different time intervals $\Delta t = 120 \ s, 1440 \ s$, respectively, that are used for computing the non-affine displacements, and the dark dashed line is a Gaussian distribution with zero mean and unit variance. Apparently, the probability distributions show strong deviations from a Gaussian distribution. We quantify this deviation from Gaussianity using the fourth
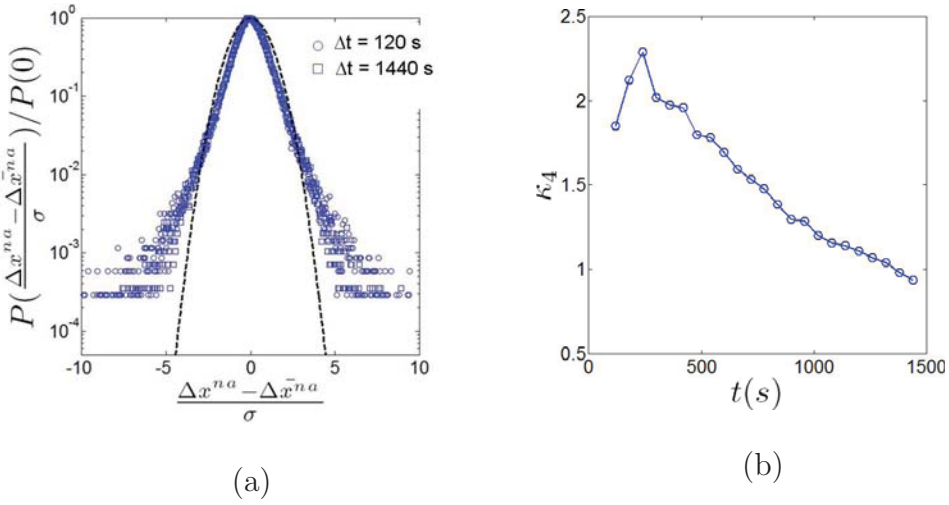
(a)   (b)

Figure 4.5: (a) Probability distribution function of the non-affine displace-
ment in the shear direction Δx^{na}, obtained at a shear rate of $\dot{\gamma} = 1 \times 10^{-5} s^{-1}$
and $\phi = 0.60$. The distribution are normalized such that the mean is zero,
the variance is unity and the maximum of the function is unity. Different
symbols denote different time intervals used for computing the non-affine dis-
placements, and the dark-dashed line is a Gaussian distribution of zero mean
and unit variance. (b) The kurtosis κ_4 of the probability distribution functions
are presented as a function of time.

moment of the distribution, which is referred as kurtosis. The kurtosis
of a distribution is defined as :

$$\kappa_4 = \left\{ \frac{1}{3N} \sum_{i=1}^{N} \left[\frac{\Delta x_i^{na} - \overline{\Delta x^{na}}}{\sigma} \right]^4 \right\} - 1, \qquad (4.8)$$

where $\overline{\Delta x^{na}}$ is the mean and σ is the standard deviation of the dis-
tribution. For a Gaussian distribution κ_4 is zero. The kurtosis of the
probability distributions of the non-affine component Δx^{na} is shown in
Fig.4.5(b) as a function of time interval. Interestingly, the kurtosis ex-
hibits a maximum at $\Delta t_m = 180\ s$, which implies that correlations are
the strongest at short times. This is related to the fact that arrested
dynamics at short time intervals give rise to strong correlations in the
system. Similar experimental observations about the probability dis-
tribution functions have been made for quiescent and sheared colloidal
glasses in other experiments [24, 115] .

4.4   Spatial correlations of shear strain and non-affine displacement

In this section, we define spatial correlations of microscopic strain and non-affine displacement to investigate the cooperative motion in sheared colloidal glasses. The spatial correlation functions of the microscopic fluctuations are defined as :

$$C_A(\delta \mathbf{r}) = \frac{\langle A(\mathbf{r} + \delta \mathbf{r}) A(\mathbf{r}) \rangle - \langle A(\mathbf{r}) \rangle^2}{\langle A(\mathbf{r})^2 \rangle - \langle A(\mathbf{r}) \rangle^2}, \tag{4.9}$$

where A is a microscopic observable, and angular brackets denote ensemble averages. A comparison of equations.(4.9) and (4.3) reveals the similarities in their definitions, and also point to the fact that local strain and non-affine displacements are the dynamic observables in our analysis. This definition allows us to visualize the spatial correlations not only as a function of distance δr, but also as a function of angle between two points. It is to be noted that the spatial correlations in glasses are time dependent because the dynamics evolve in time. They depend on the time interval δt that is used for computing shear strain and non-affine displacements and the local strain. The study of probability distributions, in the previous section, showed strongest correlation for short times. Therefore, we focus on short time dynamics to study spatial correlations.
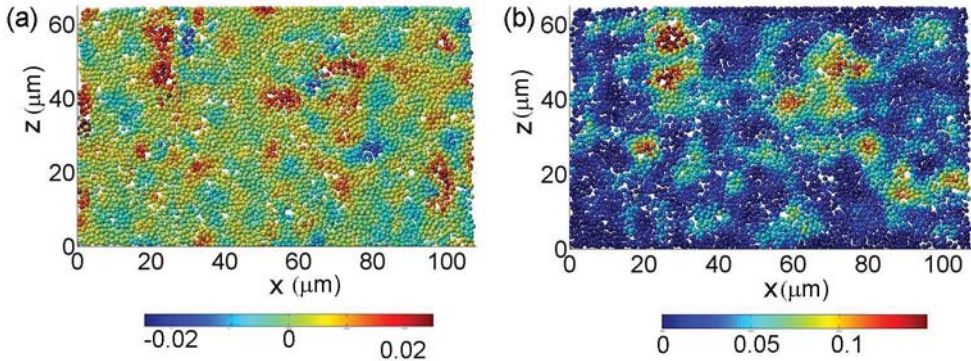

Figure 4.6: Reconstruction of shear strain ϵ_{xz} (a) and non-affine displacement D^2 (b) in a $108 \times 108 \times \sim 5 \mu m^3$ section. The ϵ and D^2 are obtained from the displacements observed over time interval of $\Delta t = 120$ s.
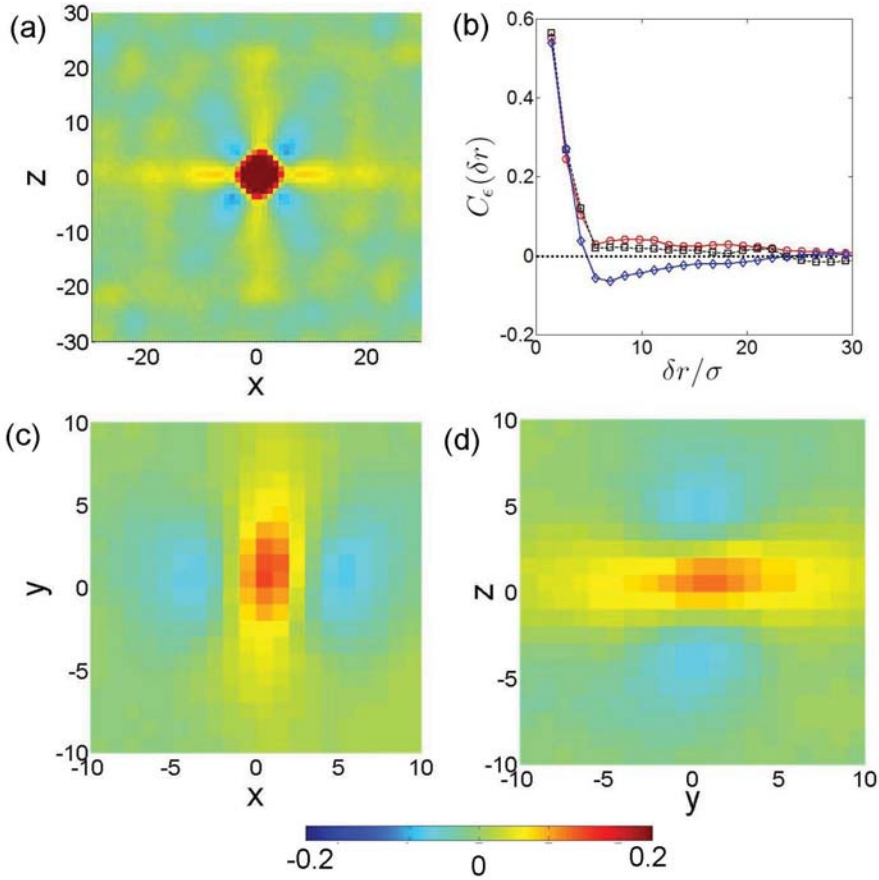
Figure 4.7: (a),(c) and (d) Color coded representations of the spatial correlation function of the shear strain C_ϵ in various planes. A section of C_ϵ in the xz plane at $y = 0$ (a), the xy plane at $z = 4$ (c) and the yz plane at $x = 4$ (d). (b) The angle dependent correlation of shear strain in the xz plane.

We first investigate the spatial correlations in the homogeneous flow that was observed at a shear rate of $\dot{\gamma} = 1 \times 10^{-5} s^{-1}$. For the convenience of understanding, we present spatial maps of the shear strain component ϵ_{xz} and D^2, in a 5 μm thick section parallel to the xz plane, in Figs.4.6(a) and (b), respectively. The network of high and low strain regions in Fig.4.6(a) is a direct consequence of the strong spatial correlations. To substantiate this point, we compute the spatial correlations of the shear strain fluctuations using Eq.4.9. Correlations in the x-z plane are obtained by taking $\delta\mathbf{r} = (\delta x, 0, \delta z)$; a corresponding color coded rep-

resentation of the correlation function $C_{\epsilon_{xz}}$ is shown in Fig.4.7(a). Remarkably, the correlation function shows a four-fold pattern at its center, which is reminiscent of the strain response of an elastic material to an ellipsoidal inclusion [86]. These observations strongly establish the elastic nature of colloidal glass, and the fact that shear transformation zones are similar to Eshelby's inclusions [86]. The angular dependence of the strain correlations in Fig.4.7(a) is apparent from the color coding. To highlight this feature, we average C_ϵ within angular wedges around the horizontal (circles), vertical(square), and diagonal(diamond) directions, and plot the corresponding angle-specific correlation function versus r in Fig.4.7(b) using different symbols.

In a similar way, we visualize the form of the correlation function C_ϵ in the xy and yz planes. Sections of the correlation function in the xy plane at $z = 4$ and the yz plane at $x = 4$ are shown in Figs.4.7(b) and (c), respectively. From the various sections, it is apparent that the central region of the correlation function, which is often referred to as inclusion, interestingly, has an ellipsoidal shape.
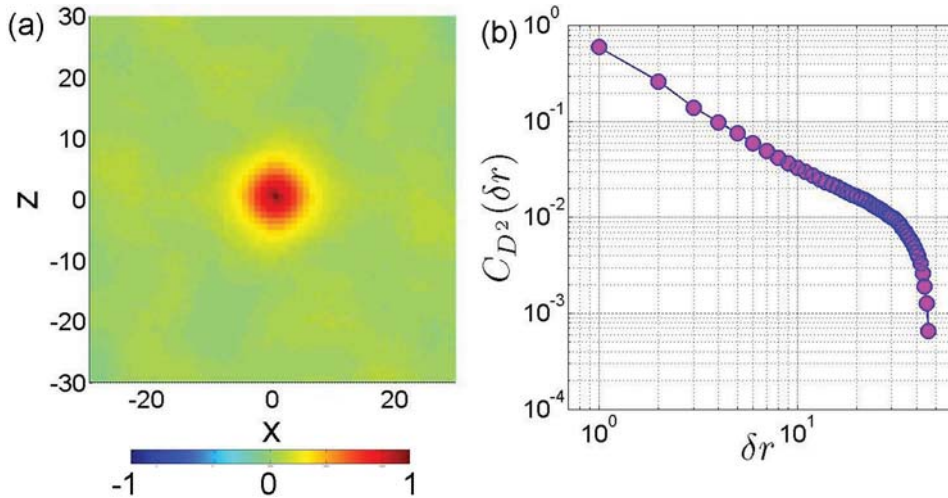

Figure 4.8: (a) A color coded presentation of the spatial correlation function of the non-affine displacement C_{D^2} in the xz plane at $y = 0$. (b) Angle-averaged correlation function $C_{D^2_{min}}$ as a function of distance δr.

We now turn our discussion to the correlation of non-affine displacements, whose spatial map in the xz plane is shown in Fig.4.6(b). As discussed earlier, the non-affine displacement is representative of the dif-

fusive motion in the system, and is a measure of plastic activity. The localized nature of the plastic deformation in the material is evident from the figure. We determine the spatial correlation function of the non-affine displacement fluctuations, C_{D^2}, using Eq. 4.9, and display a color coded representation in Fig.4.8(a). In contrast to the shear strain, the spatial correlation function of the non-affine component appears to be isotropic. So, we average the correlation function over all the angles in three dimensions, and present it as a function of distance δr in Fig.4.8(b). A remarkable power-law decay is observed, which is truncated at the vertical system size, $\delta r/\sigma \sim 50$; thus the correlations span the entire system. These results provide direct evidence of the existence of long-range dynamic correlations in a slowly flowing glass, and highlight the scale-free character of the non-affine rearrangements that gives rise to plastic deformation. The scale invariance appears to be a generic feature of elasto-plastic deformation in other materials: the dislocation motion in crystals [116, 117, 118], and the aftershocks in earth quakes [119] display similar scale-free patterns.
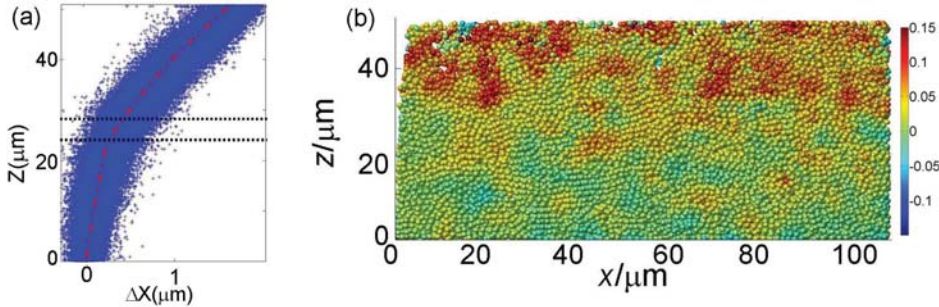

Figure 4.9: Inhomogeneous flow at $\dot{\gamma} = 1 \times 10^{-4} s^{-1}$. (a) Particle displacements along the shear direction during the time interval $\delta t = 4\ min$. Dashed red lines are linear fits to the shear profiles for $z < z_l = 23 \mu m$ (low shear band) and $z > z_h = 28 \mu m$ (high shear band). (b) A $7 \mu m$ thick reconstruction of the distribution of incremental shear strain ϵ_{xz} during the time interval $\delta t = 7\ min$.

We probe the spatial correlations of strain and non-affine displacement fluctuations by subjecting the glass to increasing shear rates. As reported in the previous chapter, the flow remains homogeneous over a range of low strain rates, however, beyond a critical strain rate of $\dot{\gamma}_c \sim 6 \times 10^{-5} s^{-1}$ we observe a sudden transition to inhomogeneous flow. The glass separates

into two bands that flow at different rates, as illustrated by the displacement profile in Fig.4.9(a), obtained at a shear rate of $\dot{\gamma} \sim 1 \times 10^{-4}s^{-1}$. A reconstruction of the shear strain distribution shows how the shear band emerges: highly non-affine shear transformations accumulate in the upper part of the glass (Fig.4.9(b)).
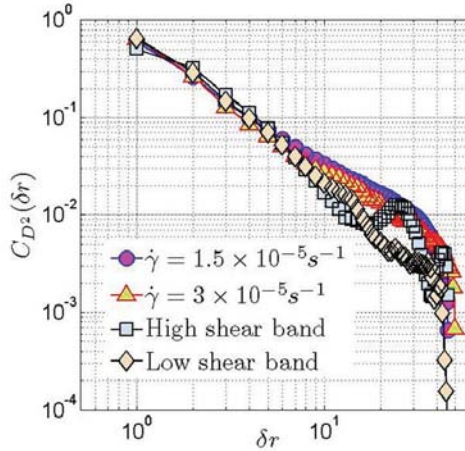

Figure 4.10:   Angle-averaged correlation function $C_{D^2_{min}}$ as a function of distance δr, for the low shear band (blue squares), the high shear band (yellow diamonds), and for the homogeneous flow at $\dot{\gamma} = 1.5 \times 10^{-5}s^{-1}$ (blue dots) and $3 \times 10^{-5}s^{-1}$ (orange triangles). A least square fit to the data gives a slope of $\alpha \sim -1.3 \pm 0.1$ (dashed line).

We investigate the robustness of the scaling observed in Fig.4.8 by determining $C_{D^2_{min}}(\delta r)$ separately for the high and low shear bands. The resulting angle-averaged correlation functions are shown together with those of homogeneous flow in Fig.4.10. A remarkable collapse of the data is observed. While the magnitude of fluctuations in the two bands differs largely, the normalized correlation function shows very similar power law decay (Fig.4.10): the same scaling exponent applies to the low and the high shear band, as well as to homogeneous flow. We find a scaling exponent of $\alpha = 1.3 \pm 0.1$ from the best fit to the data. Athermal and quasi-static shear simulations of amorphous solids [38, 39, 40, 49, 52] have shown similar long-ranged correlations; however, the effect of finite shear rate and finite temperature on the statistical correlations between shear transformations was unclear so far [120, 121, 122, 123]. Our results

conclusively show long-range correlations even at finite shear rates, and at finite temperatures.
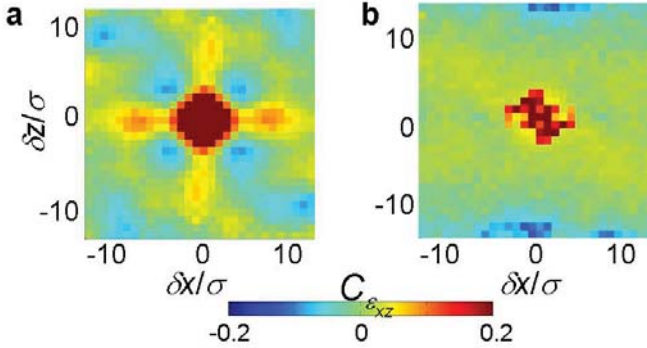

Figure 4.11:   (a) and (b) Angle-resolved spatial correlations of shear strain, $C_{\epsilon_{xz}}(\delta r)$, in the $x - z$ plane, for the low and the high shear bands shown in Fig.4.9, respectively.   Correlations are computed over a time interval of $\delta t = 3\ min$.

It is to be noted that the spatial correlations presented in Fig.4.10 were obtained using particle displacements observed over short durations. This demonstrates that the bands appear similar on short time scales. However, the fundamental difference between the two bands becomes evident when we investigate the particle dynamics as a function of time. This aspect was exploited in chapter 3 to demonstrate shear banding as the coexistence of dynamic phases. Here, we proceed along similar lines, and compute the strain correlation C_ϵ for the bands separately. Remarkably, the strain correlation function, C_ϵ reveals a symmetry change in the strain response. While for the low shear band, the central four-fold symmetry is still predominant (Fig.4.11(a)), for the high shear band, this symmetry is lost, and the pattern appears to be isotropic (Fig.4.11(b)). This symmetry change reflects the transition from a solid to a liquid-like response of the glass. A similar interpretation is given to fracture surfaces of metallic glasses that display striking evidence of such a solid to liquid transition [124]. Our colloidal glass then allows us to directly visualize the strain correlations that cause this dynamic transition.
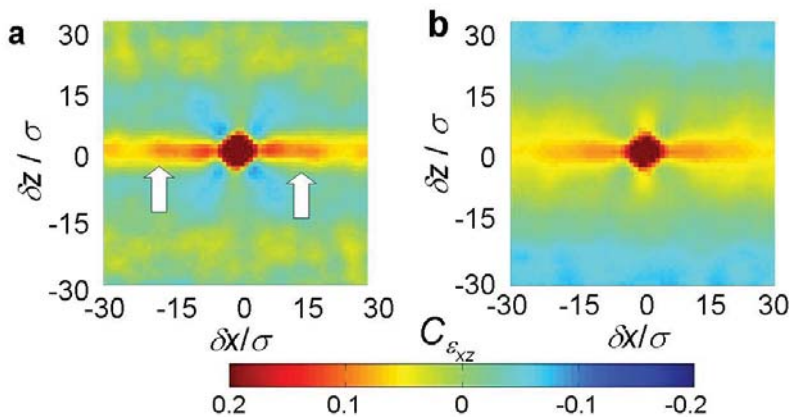
Figure 4.12: Evolution of strain correlations during shear band formation. Shear strain correlation function $C_{\epsilon_{xz}}$ before (a) and after (b) the manifestation of shear bands. The arrows in (a) indicate the strong correlation in the direction of shear that lead to shear banding in later stages (b).

4.4.1   How do shear bands emerge?

To elucidate the emergence of shear bands, we follow the spatial correlations of shear strain C_ϵ during the initial stages of shear banding (Figs.4.12(a) and (b)). The strain correlation function during the transient stage, before the shear bands manifest themselves (Fig.4.12(a), shows a strong bias in the horizontal direction. This horizontal bias signals the excitation of additional elastic modes at higher shear rates that cause strong correlations between shear transformation zones in the horizontal direction. This correlation lowers the effective resistance to flow in the direction of shear, and thereby leads to shear bands in the later stages of deformation (Fig.4.12(b)). These results highlight the importance of long-range correlations in the shear banding of glasses.

Various numerical studies of the elasto-plastic behavior of amorphous solids have focused on long-range correlations to understand the origin of shear-banding [43, 44, 125]. Bulatov and Argon [125] used a 2D model of amorphous solids, in which the plastic flow was treated as a stochastic sequence of local inelastic transformations. The model was based on the assumption that plastic flow in amorphous solids is a net result of individual plastic transformations. Their study demonstrated that the evolution of non-random internal stresses due to long-range interactions between

the shear transformations is as important as the dilatancy induced effects for understanding the formation of shear bands. Our observation of long-range spatial correlations in colloidal glasses are indeed direct experimental evidences of these ideas.

4.4.2 Scaling of different definitions of non-affine displacement
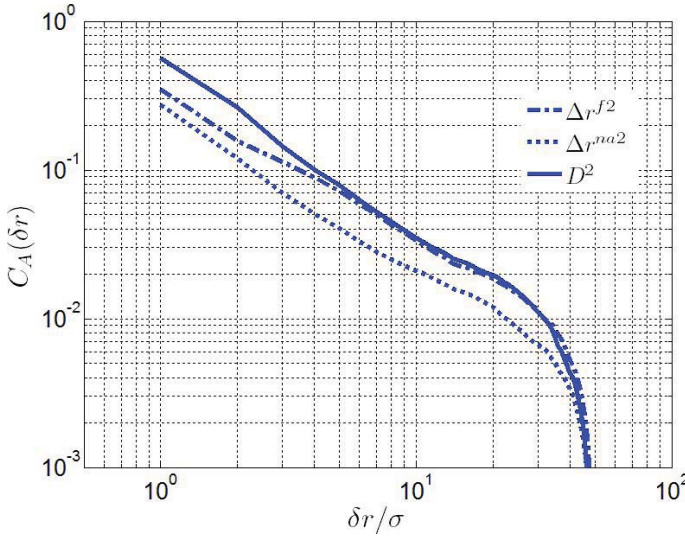

Figure 4.13: Angle averages spatial correlation of the different definitions of non-affine displacement. Different line types are used to distinguish non-affine displacements. The thick line is D^2, dash-dot line is Δr_f and dot line is Δr_{na}.

Various definitions of the non-affine displacement have been used in the literature [52]. The most prominent definition of the non-affine displacement (Δr^{na}) is based on the deviation from global deformation. The long-range nature of the spatial correlations of non-affine displacements have been confirmed in athermal, quasi-static shear simulations. Here, we compare the spatial scaling of fluctuations for various definitions of non-affine displacements. We use the definitions of non-affine displacement introduced in Chapter 2 to compute the spatial correlation functions in a homogeneously flowing glass ($\dot{\gamma} = 1.5 \times 10^{-5}s^{-1}$). Figure.4.13 shows angle-averaged spatial correlations of non-affine displacement defined by D^2 (thick line), $(\Delta r^{na})^2$ (dotted line) and $(\Delta r^f)^2$ (dash-dotted line). Sur-

prisingly, all these definitions display a similar power-law decay that is characterized by a unique exponent $\alpha = -1.2 \pm 0.1$. These observations further underline the robustness of our results.

4.5 Conclusions

Our results establish the existence of long-range spatial correlations in the flow of glasses. The four-fold symmetry of the shear strain fluctuations reveals that shear transformations are similar to Eshelby's inclusions [86]. The long-range interaction between the shear transformations gives rise to scale-free correlations in glasses. In addition, the scaling exponent remains constant over a range of shear rates, which demonstrates the robustness of our observations. These results indicate the essential importance of correlations between STZs that so far have not been taken into account in mean field theories of plasticity, which assume the random formation of STZs [37, 42, 45].

While our results for shear banding are obtained for colloidal glasses, they should be generic to glassy flows. The formation of shear bands has often been linked to strain softening of the material, caused by excess dilation, that accompanies the formation of shear transformations [41, 42]. The direct imaging of strain correlations demonstrates that long-range elastic correlations play a central role in the manifestation of such instabilities.

Finally, the robust scaling that we observe suggests a naturally scale-free flow and relaxation of glasses. We propose similar analysis of shear flows in systems like granular, foams and emulsions to test the universality of the scaling exponent, and to determine the universality class of the flow and relaxation of amorphous materials.